IBRO Neuroscience Reports 11 (2021) 119–127

Contents lists available at ScienceDirect

IBRO Neuroscience Reports

journal homepage: www.sciencedirect.com/journal/IBRO-Neuroscience-Reports

Research Paper

The effects of copper sulfate on the structure and function of the rat cerebellum: A stereological and behavioral study

Mahboobeh Erfanizadeh [a,b], Ali Noorafshan [a,b], Maryam Naseh [a,**,1], Saied Karbalay-Doust [a,b,*,2]

[a] Histomorphometry and Stereology Research Center, Shiraz University of Medical Sciences, Shiraz, Iran
[b] Anatomy Department, School of Medicine, Shiraz University of Medical Sciences, Shiraz, Iran

ARTICLE INFO

Keywords:
Copper
Cerebellum
Stereology
Rat

ABSTRACT

Copper (Cu) is a vital trace element that acts as a cofactor of proteins and enzymes in many molecular pathways including the central nervous system. The accumulation or deficiency of copper could alter neuronal function and lead to neuronal degeneration and brain dysfunction. Intake of high levels of copper can also cause copper toxicosis that affects the brain structure and function. Despite clinical and experimental data indicating the association between abnormal copper homeostasis and brain dysfunction, the effects of copper on cerebellum have remained poorly understood. Hence, this study aimed to evaluate the effects of copper sulfate on the cerebellum *via* stereological and behavioral methods in rats. Male rats (Sprague-Dawley) were divided to three groups. The rats in the control group orally received distilled water, while those in the Cu groups received 1 mM (159 mg/L) or 8 mM (1272 mg/L) copper sulfate by oral gavage solved in distilled water daily for 4 weeks. Then, the rotarod performance test was recorded and the cerebellum was prepared for stereological assessments. The Cu-administered rats (1 and 8 mM) exhibited a significant reduction in the total volumes of the cerebellum structures. The total number of the cells in the cerebellar cortex and deep cerebellar nuclei were significantly decreased *via* Cu in a dose-dependent manner. Furthermore, the length of nerve fibers and the number of spines per nerve fiber decreased significantly in the Cu groups. These changes were correlated to the animals' motor performance impairment in the rotarod test. The findings suggested that copper toxicity induced motor performance impairments in the rats, which could be attributed to its deleterious effects on the cerebellum structure.

1. Introduction

Copper (Cu) is an essential nutrient that plays a vital role in the biochemistry of whole living organisms. It acts as a cofactor of several proteins and enzymes named cuproenzymes. Copper is involved in basic mechanisms including oxygen carrying, energy production, cell metabolism, cell signaling, and hematopoiesis (Squitti and Polimanti, 2013). The average daily intake of copper in humans has been suggested to be between 0.5 and 1.5 mg, which can come from different sources such as seeds, nuts, beans, shellfish, and liver (Tapiero et al., 2003). Copper is absorbed from diet, mainly duodenum and proximal jejunum, although some of it can be absorbed in the stomach and distal part of the small intestine. It is excreted through either the gastrointestinal tract in form of absorbed and non-absorbed ions or the bile (Hordyjewska et al., 2014).

The excess of Cu in the body is referred to as copperiedus (copper toxicity) (Royer and Sharman, 2020; Taylor et al., 2020), which can occur through eating acidic foods cooked in uncoated copper utensils or receiving excessive Cu in foods, drinking water, and other environmental origins (Potera, 2004; Bost et al., 2016). Cu is also extensively used in manufacturing industries, electronic products, and agrochemicals (Newhook et al., 2003; Arnal et al., 2011).

Cu is present in different regions of the brain such as hippocampus, basal nuclei, cerebellum, and numerous synaptic membranes (Kozma et al., 1981; Madsen and Gitlin, 2007; Popescu et al., 2009). Alterations in Cu homeostasis affect the Central Nervous System (CNS), which can

* Corresponding author at: Histomorphometry and Stereology Research Center, Shiraz University of Medical Sciences, Zand Ave., 71348-45794 Shiraz, Iran.
** Corresponding author.
E-mail addresses: naseh@sums.ac.ir (M. Naseh), karbalas@sums.ac.ir (S. Karbalay-Doust).
[1] ORCID ID: https://orcid.org/0000-0003-4254-5175
[2] ORCID ID: https://orcid.org/0000-0003-1071-1730

https://doi.org/10.1016/j.ibneur.2021.09.001
Received 4 April 2021; Received in revised form 1 September 2021; Accepted 10 September 2021
Available online 15 September 2021

lead to neurological disorders (Gaggelli et al., 2006; Desai and Kaler, 2008). It has been found that chronic Cu toxicity caused differential copper buildup in the cortex, striatum, and cerebellum regions in male Wistar rats, which was associated with cognitive dysfunctions (Pal and Prasad, 2016). It was also reported that Cu overload through oral administration increased the amounts of nonceruloplasmin-bound Cu (free-Cu) in plasma, cortex, and hippocampus, which could induce oxidative damage through the overproduction of Reactive Oxygen Species (ROS) (Arnal et al., 2013). It seems that the oxidative stress is the main reason for the neurological deficits following Cu accumulation (Tapiero et al., 2003; Özcelik et al., 2012).

Cerebellum is critically involved in balance, motor control, and different brain functions including emotional regulation and cognition (Baldaçara et al., 2008; Sathyanesan et al., 2019). Since the cerebellum is one of the brain areas vulnerable to copper toxicity, it is reasonable to assume that the elevation of Cu concentration in the cerebellum may affect its structure and function.

Methods of stereology are increasingly applied for the determination a variety of morphometric variables of three dimensional structures. To the best of our knowledge, no studies have evaluated the effects of copper sulfate on the rat cerebellum model using stereological methods and to obtain the quantitative histological data.

Thus, the present research aims to evaluate whether the excessive intake of copper sulfate may affect structural parameters. For this purpose, the volume of different parts of the cerebellum, the number of different types of cerebellar cells, the length of nerve fibers, and the number of spines per nerve fibers in the cerebellum were evaluated by stereological methods. Additionally, motor performance was assessed using the rotarod test in order to evaluate cerebellar dysfunction.

2. Materials and methods

2.1. Animals

In the present study, 24 adult male Sprague-Dawley rats (170–230 g) were obtained from the Center of Comparative and Experimental Medicine of Shiraz University of Medical Sciences, Shiraz, Iran. All procedures were performed according to the guidelines of the Ethics Committee of Shiraz University of Medical Sciences (approval No. 91-6416).

The rats were maintained in a standard room with a 12/12 h light-dark period, temperature of 22 ± 2 °C, and humidity of 50%. Additionally, the animals had access to both food and water *ad libitum*.

2.2. Experimental design

After a week of acclimatization, the animals were randomly divided to three groups (n = 8). All eight rats in each group underwent rotarod test examination and six rats per group were evaluated by stereological techniques (Hyde et al., 2007). The rats in the control group received distilled water by oral gavage, while those in the copper groups received 1 mM (159 mg/L) or 8 mM (1272 mg/L) copper sulfate (Catalog Number: 102790, Sigma-Aldrich, Germany) by oral gavage, solved in distilled water daily for 4 weeks. After 4 weeks, motor performance was evaluated by the rotarod test and the right cerebellar hemisphere was used for stereological investigation.

2.3. Rotarod test for evaluation of motor skill performance

The rats were pre-trained on the rotarod apparatus at a speed of 15 rpm for 60 s over two consecutive days. They were tested on the fixed speed first and on the accelerating rotarod 2 days later. Accordingly, the rats were tested at seven different speeds; *i.e.*, 12, 16, 19, 21, 24, 26, 28, and 38 rpm, for 60 s at each speed. It should be noted that the trials were performed three times at each speed with 20-min intervals. After that, they were placed on the rod at the speed of 5–45 rpm for 300 s. The latency to fall was recorded, as well (Monville et al., 2006).

2.4. Preparation of tissues

The brains were fixed by cardiac perfusion using 4% paraformaldehyde solution. After removing the cerebellum and paraffin embedding, paraffin blocks were serially sectioned coronally with 25 μm thickness and were stained by the Cresyl violet method. Then, 10–12 sections were selected in each rat according to systematic uniform random sampling. The image of each section was evaluated at the final magnification of 23× by using a video microscope and the stereology software designed at the university.

2.5. Estimation of the volumes of the cerebellar hemisphere, cortex, the white matter of the medulla, and deep cerebellar nuclei

The total volumes of the cerebellar hemisphere, cortex was estimated using the Cavalieri method. For this purpose, twenty six μm thickness coronal sections from right hemispheres were prepared and stained with Cresyl violet. Among these sections, 10–12 were selected through systematic uniform random sampling to estimate the total volume of the cerebellar hemisphere and cortex. Another set of 10–12 sections were also sampled containing deep cerebellar nuclei. The lateral, interposed, and medial nuclei were considered collectively as the deep cerebellar nuclei.

The stereological tools included stereomicroscope joined to a computer, at the final magnification of 23× by the point- counting software designed at the Histomorphometry and Stereology Research Center of the Shiraz University of Medical Sciences. The probes of stereology were superimposed on the live images and the volume was estimated by point-counting method (Gundersen et al., 1988; Kristiansen and Nyengaard, 2012). Also, the distances between the sampled sections (d) were calculated. Besides, area was evaluated using point-counting method. Accordingly, the area per point (a/p) was 0.84 mm^2 and averagely 150–250 points ($\sum P$) were counted per animal. Finally, the volume was evaluated using the following formula:

$$V = (a/p) \times \sum P \times d$$

2.6. Estimation of the numbers of Golgi, Bergman, Granule, and Purkinje cells, neurons, and glial cells

A light microscope (Nikon E200, Japan) with an oil immersion lens (60×) with the numerical aperture of 1.4 linked to a computer was applied to evaluate the total number of the cells through the optical disector technique. The microscopic fields were selected by moving the microscope stage in an equal distance based on systematic uniform random sampling (Gundersen et al., 1988; Kristiansen and Nyengaard, 2012). The MT12 microcator (Heidenhain, Germany) installed on the stage was used to measure the Z-axis movement of the microscope stage (Gundersen et al., 1988; Kristiansen and Nyengaard, 2012). The unbiased counting frame with the area per frame (a/f) of 850 μm^2 and acceptance (right and upper) and forbidden (left and lower) lines was superimposed on the images of the sections displayed on the monitor. The Z-axis distribution was plotted to obtain the guard area and the height (h) of the disector (von Bartheld, 2012). Accordingly, the counted cells from the 0–100 percentiles were grouped into 10 bins *via* the histological tissue height from the upper (0%) to the lower surface (100%). The Z-axis distribution of the nuclei has been shown in Fig. 1a. The upper 10% and lower 30% were considered guard zones and were ignored due to the histogram, and cell counting was done in the remaining 40% (h) (von Bartheld, 2012). Any cell nucleus coming into focus in the sampling box ($a/f \times h$) was selected if it was located totally or partly inside the counting frame and did not touch the forbidden lines

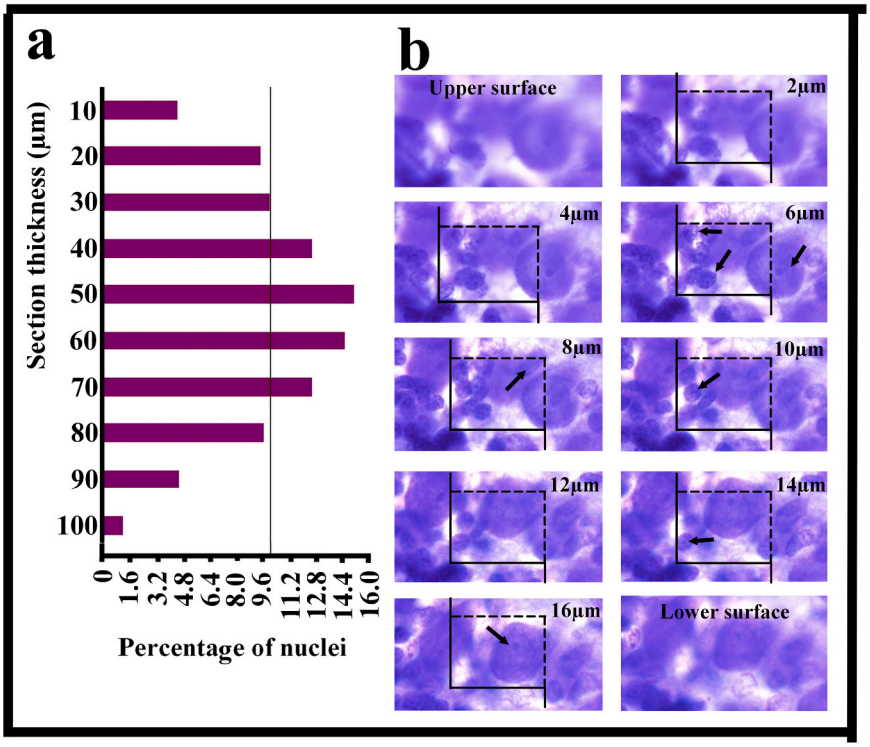

Fig. 1. The plot presentation of Z-axis distribution of the cerebellar cells' nuclei was used to select the disector's height and appropriate guard zones. The counted cells were scored and divided into 10 histograms from the 0–100 percentiles throughout the tissue section. The horizontal line shows how the nuclei would present if distribution of all visible nuclei was equal through the Z-axis (a). The optical disector method was used to estimate the numerical density of different cerebellar cells. A selected image of microscopic field at the upper surface of the tissue section, at eight successive focal planes below the upper surface with a distance of 2 µm between the focal planes, and at the lower surface of the tissue section that was found 18 µm below the upper surface. Between 2 µm and 16 µm, an unbiased counting frame was superimposed on the images of the tissue sections stained with cresyl violet. The cerebellar cells' nuclei becoming visible through scanning of the height of the disector were counted by the unbiased counting frame (arrow) (b).

(Fig. 1b). The total number of the cells was calculated *via* multiplying the numerical density (Nv) by the total volume of the cortex or the deep cerebellar nuclei.

$$Nv\ (cells) = [\sum Q/\sum p \times (a/f) \times h] \times t/BA$$

Where (ΣQ) represented the total number of the cells that came into focus during movement towards the height of the disector, (ΣP) was the total number of the associated points in all frames, (h) was the height of the disector, (a/f) was the frame area, (t) was the mean section thickness (23 µm), and (BA) was the block advance of the microtome (25 µm) (Gundersen et al., 1988; Kristiansen and Nyengaard, 2012).

2.7. Estimation of the length of the fibers

Vertical Uniform Random (VUR) sectioning is necessary for estimation of fibers' length (Noorafshan et al., 2015). Briefly, a trocar or needle (1 mm diameter) was pushed vertically to the pial surface of the cerebellar cortex to punch out 9–10 cylindrical cortical tissues (Fig. 2a). The cylindrical tissues were then randomly turned around parallel to the vertical axes and were collectively embedded in the paraffin block. The sections with the thickness of 100 µm were obtained by a microtome and were evaluated using a microscope (Nikon E-200, Japan) fortified with the 100× objective lens and numerical aperture of 1.4 connected to a computer. The counting frame was then superimposed on the monitor image as well as a cycloid grid. The grid was oriented to the vertical axis of the cylinder in parallel (Fig. 2b). The number ($\sum Q^-$) of the Purkinje cell bodies and the total number of the intersections ($\sum I$) between the nerve fibers' axes and the cycloids were counted *via* the optical disector method (Fig. 2b) using the following formula:

$$I_N = 2 \times a/l \times 1/asf \times M^{-1} \times \sum I/\sum Q^-$$

Where (a/l) was the area per cycloid test length, (asf) was the area related to the cycloid grid divided by the area of the counting frame, and (M) was the final magnification (4000×). The following formula was used to obtain the mean length of the nerve fibers per Purkinje cell:

$$I_N = \text{total dendritic length / total number of neurons}$$

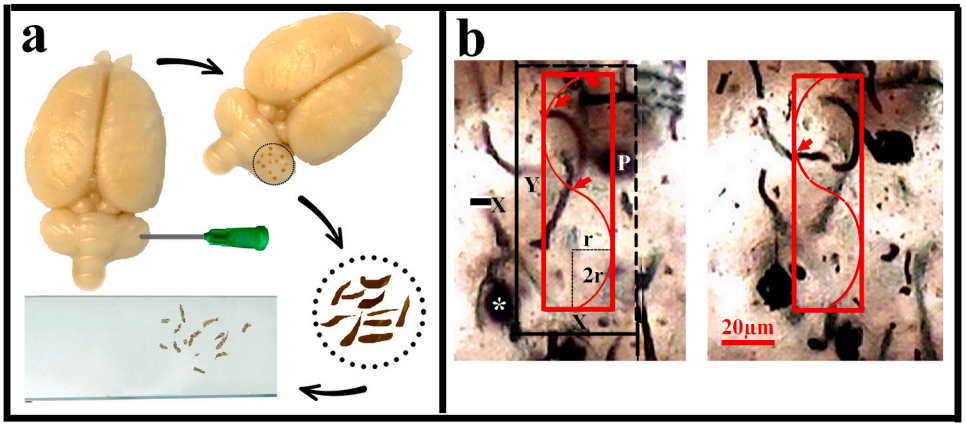

Fig. 2. The estimation of the length of the nerve fibers in the cerebellar cortex per Purkinje cell. The tissue cylinders were punched out from the cerebellum using a trocar vertical to its pial surface (a). The cylindrical tissue was mounted on a slide (a). Four cycloids were designed and located at a quadrangle (b). The length of each cycloid was obtained by twice of the length of the lesser axis (r). The area of the cycloid was calculated by multiplying X by Y. The number of the Purkinje cells was counted using the counting frame (the large frame). The total number of the intersections between the fibers' axes and the cycloids was counted (the arrows) (b).

2.8. Estimation of the numerical density and the dendritic spines morphology

The dendritic spines were identified as the small bulges less than 3 μm extended out from the main dendrite. The bulge without expansion was assumed as a thin spine. However, the bulge was classified as a stubby or mushroom spine if it displayed a stubby or mushroom expansion in its tip. It should be mentioned that the dendritic protrusions in the main dendrites were counted and expressed as the number of spines per 10 μm dendritic length (Noorafshan et al., 2018).

2.9. Estimation of the coefficient of error (CE)

The Coefficient of Error (CE) in the volume and number estimations was estimated as explained previously (Deniz et al., 2018). The CE of the volume and number of neurons varied from 0.03 to 0.06.

2.10. Statistical analysis

The values have been shown as mean ± standard error (mean- ± SEM). After assessment of the normal distribution of the data, statistical significance for stereological parameters was determined using Kruskal-Wallis H test followed by Mann–Whitney *U* test. Besides, two-way ANOVA followed by post-hoc Tukey was used to estimate the motor performance of the rats in the rotarod test. $P < 0.05$ was considered statistically significant.

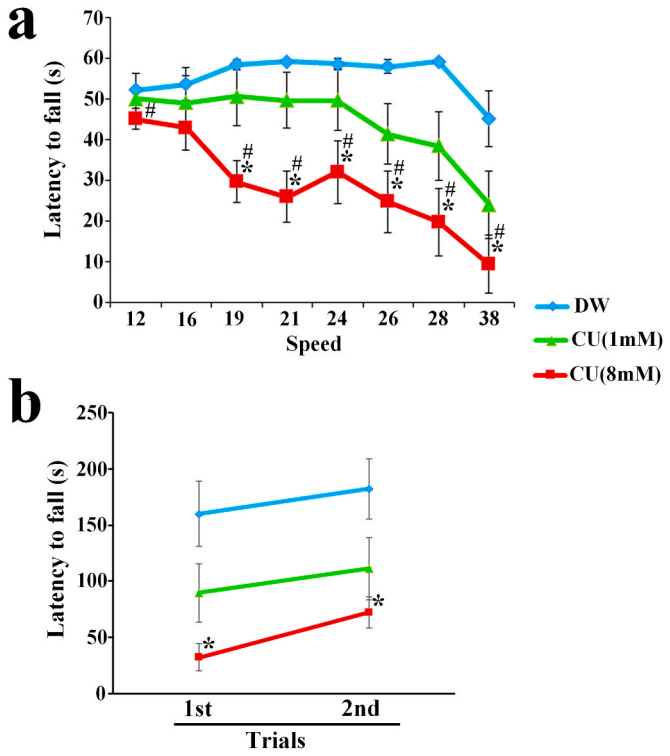

Fig. 3. The effects of distilled water (DW) and Cu (1 or 8 mM) treatments on the rats' motor performance in the rotarod test; upper: fixed speed test, lower: accelerating speed test. *$p < 0.01$ *vs.* DW, # $p < 0.01$ *vs.* CuSo4 (1 mM) (a and b).

3. Results

3.1. Rotarod performance

On the fixed-speed rotarod, 8 mM Cu-treated rats fell off significantly earlier compared to the animals in the distilled water group (Fig. 3a). In addition, the mean ± SEM of the endurance or riding time (seconds) was significantly shorter in the 8 mM Cu-treated rats compared to the distilled water group (19 rpm: 28.9 ± 3.89, 21 rpm: 33 ± 5.83, 24 rpm: 26 ± 6.4, 28 rpm: 39 ± 7.42, and 38 rpm: 35 ± 0.43; $p < 0.01$) as well as to the 1 mM Cu-treated rats (12 rpm: 42 ± 2.18, 19 rpm: 20 ± 0.34, 21 rpm: 21 ± 2.75, 24 rpm: 26 ± 5.85, 26 rpm: 34 ± 7.37, 28 rpm: 30 ± 1.6, and 38 rpm: 30 ± 1.79; $p < 0.01$). Riding time (seconds) was similar in the 1 mM Cu-treated rats and the distilled water group.

The latency to fall was significantly lower in the 8 mM Cu-treated rats than in the distilled water group in the first and second trials of the accelerating speed rotarod test (79.75% *vs.* 60.24%) (Fig. 3b). However, no significant difference was found between the 1 mM and 8 mM Cu-treated rats in this regard.

3.2. Estimation of the volumes of the cerebellar hemisphere, cortex, and the white matter of medulla

The total volumes of the cerebellar hemisphere and cortex reduced by 22% and 29%, respectively in the 1 mM and 8 mM Cu-treated rats in comparison to the distilled water group ($p = 0.002$). However, no significant difference was observed between the 1 mM and 8 mM Cu-treated groups in this regard (Fig. 4a, b, and c). Furthermore, the total volume of the medullary white matter reduced by 40% in the 8 mM Cu-treated rats in comparison to the distilled water group ($p = 0.004$). Moreover, the total volume of the medullary white matter significantly reduced in the 8 mM Cu-treated rats compared to the 1 mM Cu-treated ones ($p = 0.026$).

3.3. Estimation of the deep cerebellar nuclei volume

The total volume of the deep cerebellar nuclei was decreased by 28% and 30% in the animals treated with 1 mM and 8 mM Cu, respectively compared to the distilled water group ($p = 0.002$). There was also a significant difference between the 1 mM and 8 mM Cu-treated groups in this regard ($p = 0.043$) (Fig. 4d).

3.4. Estimation of the number of cells in the cortex of the cerebellum

The total number of Golgi cells in the cortex of the cerebellum was reduced by only 8% (not significant), while the number of Bergman cells (40%, $p = 0.004$), Granule cells (44%, $p = 0.002$), Purkinje cells (12%, $p = 0.026$), neurons (39%, $p = 0.008$), and glial cells (37%, $p = 0.002$) reduced significantly in the 1 mM Cu-treated rats compared to the distilled water group (Fig. 5a, b, and c; Fig. 6a, b, and c). Additionally, the total number of the Golgi, Bergman, Granule, and Purkinje cells, neurons, and glial cells reduced by 36%, 57%, 41%, 62%, 60%, and 51%, respectively in the 8 mM Cu-treated rats compared to the distilled water group ($p = 0.002$) (Fig. 5a, b, and c; Fig. 6a, b, and c). Moreover, a significant reduction was observed in the number of Golgi cells ($p = 0.002$), Bergman cells ($p = 0.008$), Granule cells ($p = 0.004$), Purkinje cells ($p = 0.002$), neurons ($p = 0.008$), and glial cells ($p = 0.041$) in the 8 mM Cu-treated group compared to the 1 mM Cu-treated group (Fig. 5a, b, and c; Fig. 6a, b, and c).

3.5. Estimation of the number of cells in the deep cerebellar nuclei

The total number of the glial cells in the deep cerebellar nuclei decreased by 26% in the animals treated with 1 mM Cu in comparison to the distilled water group ($p = 0.026$). However, no significant reduction was detected in the total number of neurons in the deep cerebellar nuclei

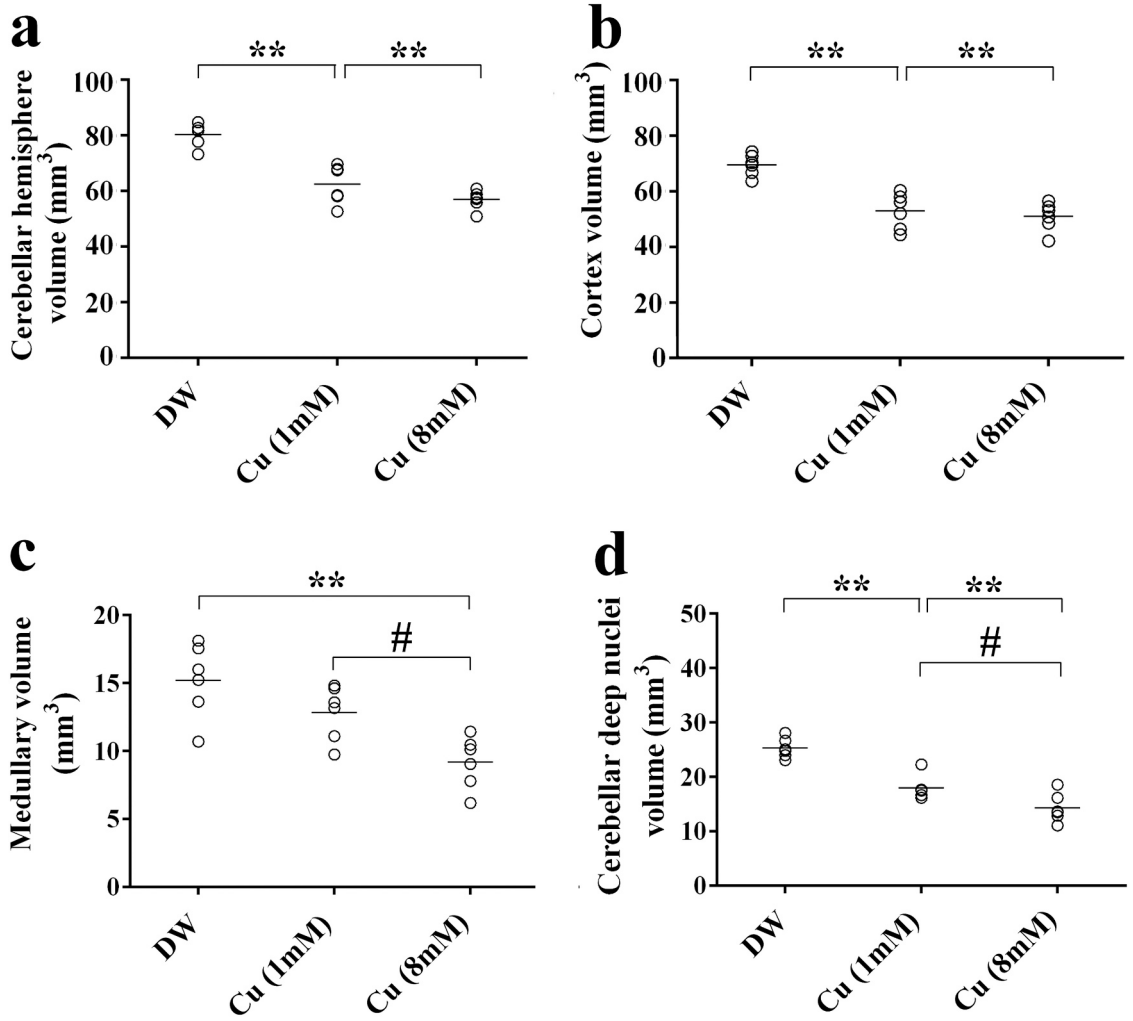

Fig. 4. The dot plots of the total volumes of the cerebellar hemisphere (a), cortex (b), medullary white matter (c), and deep cerebellar nuclei (d) in distilled water (DW) and Cu-treated (1 or 8 mM) groups. Each dot represents an animal and the horizontal bar is the average of the parameter. **p < 0.01 *vs.* DW.

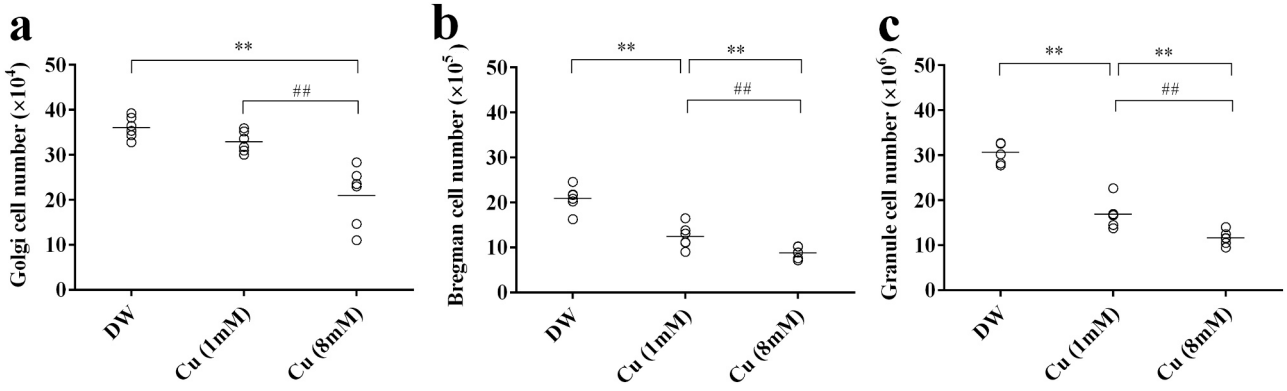

Fig. 5. The dot plots of the total number of the Golgi (a), Bergman (b), and granule cells (c) in distilled water (DW) and Cu (1 or 8 mM) groups. Each dot represents an animal and the horizontal bar is the average number of animals in each group. **p < 0.01, *p < 0.05 *vs.* DW, ## p < 0.01, # p < 0.05 *vs.* CuSo4 (1 mM).

in the 1 mM Cu-treated animals compared to the distilled water group (Fig. 7a and b). Furthermore, the total number of the neurons and glial cells in the deep cerebellar nuclei reduced by 46% and 51%, respectively in the animals treated with 8 mM Cu compared to the distilled water group ($p = 0.002$ and $p = 0.004$, respectively) (Fig. 7a and b). This index was found to be significantly lower in the 8 mM Cu-treated group compared to the 1 mM Cu-treated group ($p = 0.015$ and $p = 0.037$, respectively) (Fig. 7a and b).

3.6. Estimation of the length of the nerve fibers in the cerebellar cortex

The results indicated that the mean length of the nerve fibers of the cerebellar cortex respectively reduced by 14% and 18% in the 1 mM and 8 mM Cu-treated groups compared to the distilled water group

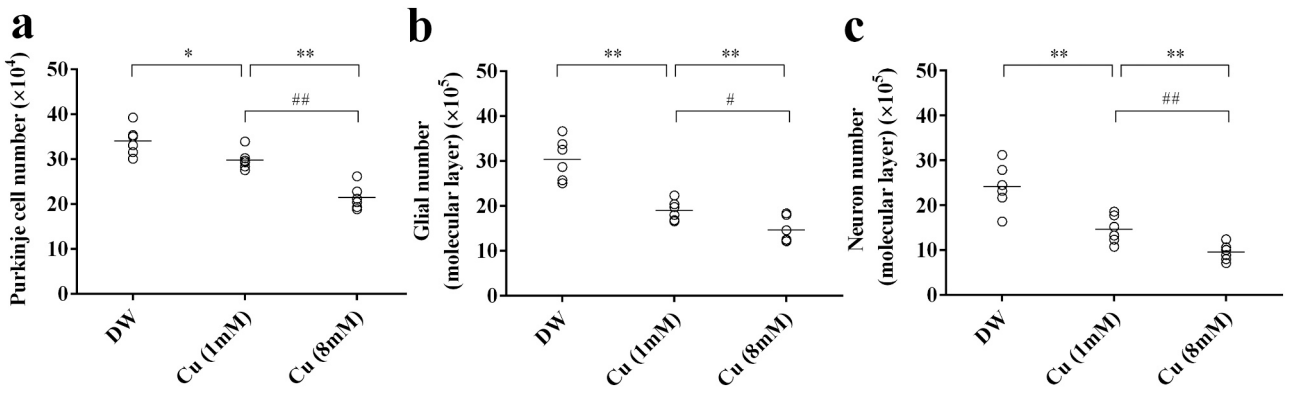

Fig. 6. The dot plots of the total number of Purkinje cells (a), glial cells (b), and neurons (c) of the molecular layer in distilled water (DW) and Cu (1 or 8 mM) groups. Each dot represents an animal and the horizontal bar is the average number of animals in each group. **p < 0.01, *p < 0.05 *vs.* DW, ## p < 0.01, # p < 0.05 *vs.* CuSo4 (1 mM).

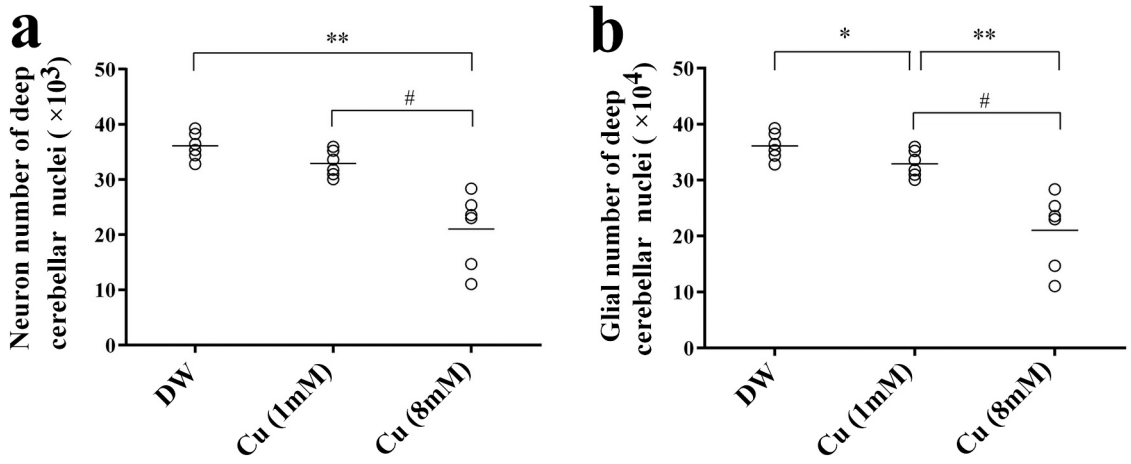

Fig. 7. The dot plots of the total number of neurons (a) and glial cells (b) of the deep cerebellar nuclei in distilled water (DW) and Cu (1 or 8 mM) groups. Each dot represents an animal and the horizontal bar is the average number of animals in each group. **p < 0.01, *p < 0.05 *vs.* DW, # p < 0.05 *vs.* CuSo4 (1 mM).

(p = 0.041) (Fig. 9a). Similarly, this index reduced significantly in the 8 mM Cu-treated group compared to the 1 mM Cu-treated group (p = 0.041) (Fig. 8a).

3.7. Estimation of the number of spines per nerve fiber

The mean number of the thin spines per total nerve fibers respectively decreased by 9% and 22% in the 1 mM and 8 mM Cu-treated groups compared to the distilled water group (p = 0.03 and p = 0.002, respectively). Moreover, the mean number of the thin spines per total nerve fibers reduced to a more extent in the 8 mM Cu-treated group compared to the 1 mM Cu-treated group (p = 0.026). The mean number of the stubby spines per total nerve fibers also decreased by 46% and 51% in the 1 mM and 8 mM Cu-treated groups, respectively compared to the distilled water group (p = 0.008 and p = 0.006, respectively). Additionally, the mean number of the mushroom spines per total nerve fibers decreased by 21% and 14%, respectively in the 8 mM Cu-treated group compared to the distilled water and the 1 mM Cu-treated groups (p = 0.002). Nonetheless, no statistically significant reduction was found in the 1 mM Cu-treated rats compared to the distilled water group. According to the findings, the maximum loss was observed in the stubby spines after treatment with 1 or 8 mM Cu (Fig. 8b, c, and d).

3.8. Quantitative evaluation

The photomicrographs of the cerebellar cortex and deep cerebellar nuclei in different groups have been depicted in Fig. 9. Briefly, the quantitative results indicated that the cells population in the cerebellar cortex and deep nuclei reduced in the 1 and 8 mM Cu-treated animals in comparison to the distilled water group. It should also be noted that a more extensive reduction was seen in the 8 mM Cu-treated group (Fig. 9a, b, and c).

4. Discussion

This study indicated for the first time that excessive consumption of copper sulfate had unfavorable effects on the cerebellum structure and function in the rat model. The first part of the study demonstrated that 1 or 8 mM Cu treatment for 4 weeks induced major structural changes in the cerebellum including the loss of the cerebellar volume and its structures, loss of different cell populations, reduction of the length of the nerve fibers, and decline in the number of spines per nerve fiber. In this study, the stereological method was used. The advantage of by stereological method is obtaining unbiased and precise estimations. Interestingly, the results demonstrated that the effect of Cu treatment was dose-dependent and the deleterious effects were more extensive in the higher dose.

Evidence has suggested that Cu homeostasis alterations could affect the CNS and cause numerous neurological and neurodegenerative

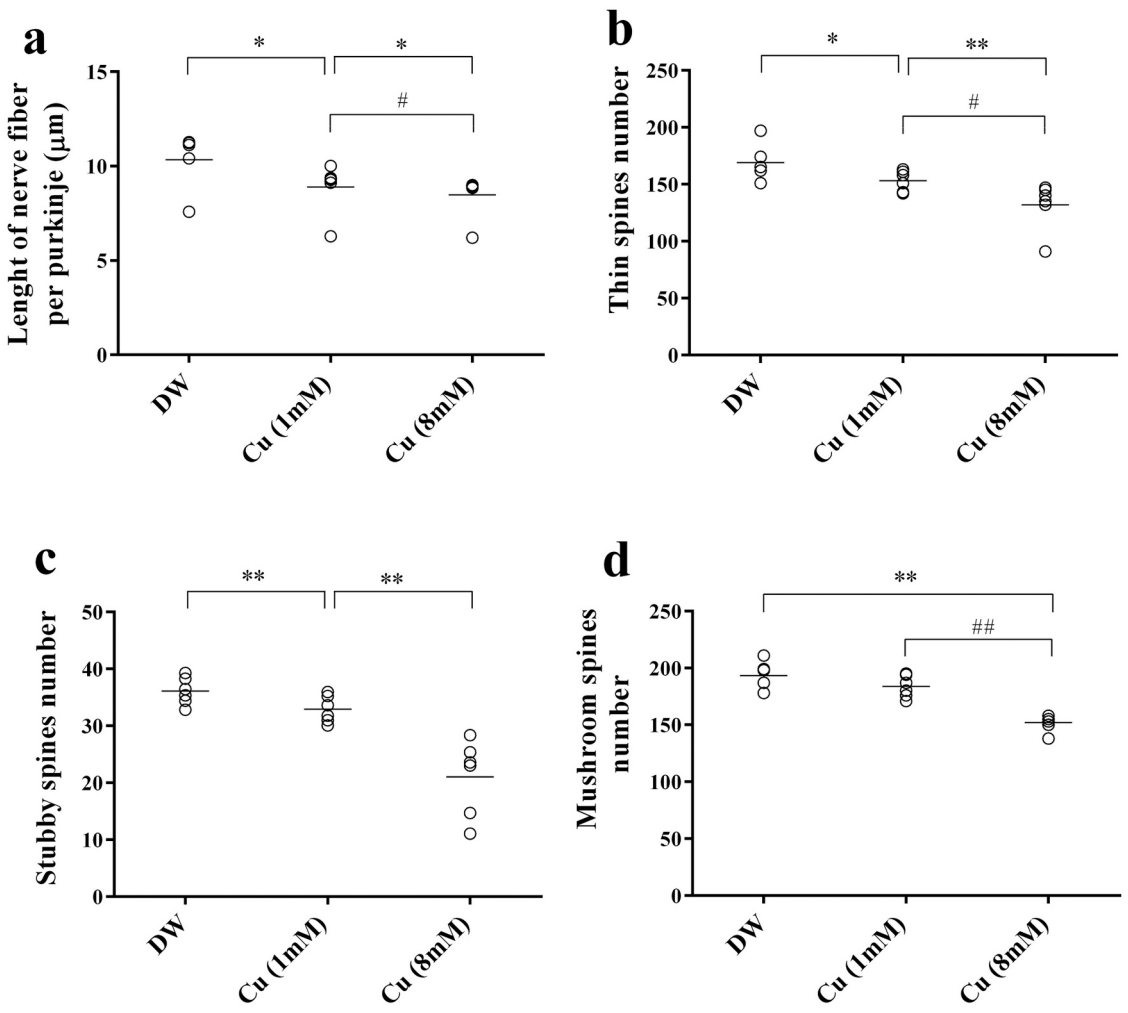

Fig. 8. The dot plots of the nerve fibers. The length of the nerve fibers (a) and the number of thin spines (b), stubby spines (c), and mushroom spines (d) per Purkinje cell in distilled water (DW) and Cu (1 or 8 mM) groups. Each dot represents an animal and the horizontal bar is the average of the parameter. **p < 0.01, *p < 0.05 *vs.* DW, ## p < 0.01, # p < 0.05 *vs.* CuSo4 (1 mM).

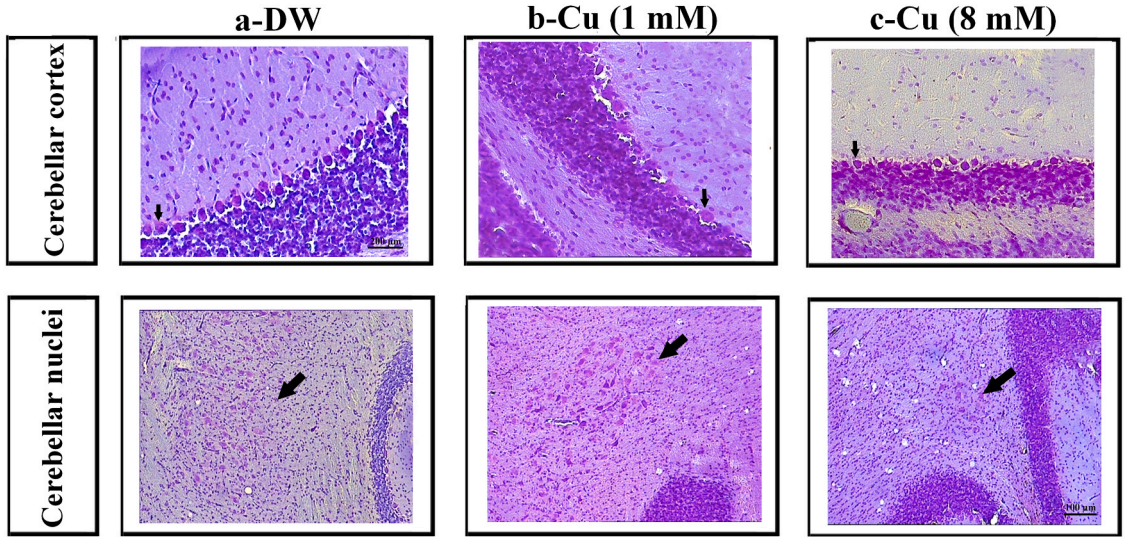

Fig. 9. A micrograph presenting the cerebellar cortex and cerebellar nuclei of the rats in distilled water (a), 1 mM CuSo4 (b), and 8 mM CuSo4 (c) groups. The population of the cells in the cortex decreased more extensively in the 8 mM Cu-treated group than in the 1 mM Cu-treated group. The arrows indicate the Purkinje cells and the nuclei's cells. Cresyl violet staining.

diseases (Gaggelli et al., 2006; Desai and Kaler, 2008). Some clinical studies have shown that excess of Cu in some diseases resulted in structural changes in different areas of the brain including caudate nucleus, globus pallidus, thalamus, cerebellum, and cerebral cortex (Stezin et al., 2016; Smolinski et al., 2019). However, few experimental data are available regarding the volumetric changes and neuronal loss induced by Cu toxicity in different vulnerable brain regions. It has been observed that copper overdose together with ethanol intake could cause neuronal loss in the subdivisions of hippocampus in rats' brains (Turgut et al., 2003). In addition, Cu toxicity could induce apoptosis and astrocytosis of the brain regions including hippocampus and frontal cortex through direct or glutamate and oxidative stress pathways, eventually leading to impaired memory and learning (Kalita et al., 2018).

Prior studies have indicated that impairment of Cu homeostasis could induce neuronal death and synaptic alterations *via* decreasing neuronal viability (Sadiq et al., 2012; Opazo et al., 2014). The diminution in the volume of the cerebellum and its structures following Cu toxicity could also be ascribed to cell reduction.

In addition to structural changes, alterations of spontaneous and evoked activities of neurons within the cerebellar network and long-lasting synaptic processes like long-term potentiation and depression could result from Cu-induced neurotoxicity, especially through oxidative damages to the cerebellar neurons (Kapkaeva et al., 2017). It has been demonstrated that copper overload in Wilson's disease could cause CNS damage *via* increasing the generation of free radicals and mitochondrial dysfunction (Schilsky, 2009). It has been also shown that oxidative stress might be responsible for structural changes and neurological deterioration induced by increasing the free serum copper (Ranjan et al., 2015).

The second part of the current study revealed the unfavorable effects of copper sulfate on motor skill performance. The behavioral impairment might be associated with the changes in the cerebellum structure, which resulted from toxicity due to Cu treatment. Previous studies postulated that brain volume reduction was associated with motor impairment in different neurological diseases (Guevara et al., 2016; Nakamura et al., 2018). The current study results were in line with the above-mentioned findings and indicated that the neurotoxic effects of Cu led to a reduction in the volume and number of the cells in the cerebellum, which were correlated to motor impairment. Furthermore, the present study showed that Cu treatment in both doses could dramatically reduce the length of the nerve fibers and the number of spines per nerve fiber, especially in the 8 mM Cu-treated group, which might be another cause of motor function impairment. Dendritic spines are the small protruding structures on the surfaces of dendrites that act as postsynaptic compartments in excitatory synapses. The spine plasticity is related to learning and memory function (van der Zee, 2015). Additionally, the number of dendritic spines is closely associated with motor performance during the early stages of learning (Xu et al., 2009), and the survival of new spines is correlated to the retention of motor skills (Yang et al., 2009). Therefore, the corresponding data led to the notion that reduction in the number of spines could induce motor skill impairment. It has also been observed that copper-induced neuronal injury was accompanied by behavioral changes in the animal model of Wilson's disease (Przybyłkowski et al., 2013). Motor and cognitive disturbances were also detected in the Wilson's disease mouse model, which might result from inflammatory mechanisms following Cu toxicity (Terwel et al., 2011). Hence, inflammatory signaling could be another possible mechanism, which is recommended to be assessed in future investigations.

The present study had many limitations. Firstly, the amount of copper concentration in the cerebellum has not been measured. Secondly, other areas of the brain such as basal ganglion have not been examined at the same time as the cerebellum.

In conclusion, Cu treatment induced major structural changes in the cerebellum including a reduction in the volumes of the cerebellum and its structures, loss of different cell populations, reduction in the length of the nerve fibers, and decline in the number of spines per nerve fiber in a dose-dependent manner. These changes led to motor performance impairment in the rats in the rotarod test.

Funding

The study was financed by grant No. 91-6416 from Shiraz University of Medical Sciences, Shiraz, Iran.

Ethics statement

All procedures in this experiment were performed in accordance with the guidelines pertaining to the Care and Use of Laboratory Animals (National Academy Press, 1996, Washington, USA) and were approved by the Ethics Committee of Shiraz University of Medical Sciences (approval No. 91-6416).

CRediT authorship contribution statement

A. Noorafshan: Conceptualization, Methodology, Software. **M. Erfanizadeh**: Practical work and data collection. **M. Naseh**: Data analysis, Data curation, Writing and editing the article. **S. Karbalay-Doust**: Validation and writing, reviewing, and editing the manuscript.

Acknowledgments

This research was a part of Mahboobeh Erfanizadeh's M.Sc. thesis in Anatomy and was financially supported by grant No. 91-6416 from Shiraz University of Medical Sciences, Shiraz, Iran. Hereby, the authors would like to thank Ms. A. Keivanshekouh at the Research Consultation Center (RCC) of Shiraz University of Medical Sciences for improving the use of English in the manuscript.

Conflicts of Interest

The authors declare that they have no conflict of interests.

References

Arnal, N., Astiz, M., de Alaniz, M.J., Marra, C.A., 2011. Clinical parameters and biomarkers of oxidative stress in agricultural workers who applied copper-based pesticides. Ecotoxicol. Environ. Saf. 74, 1779–1786.

Arnal, N., Castillo, O., de Alaniz, M.J., Marra, C.A., 2013. Effects of copper and/or cholesterol overload on mitochondrial function in a rat model of incipient neurodegeneration. Int. J. Alzheimer's Dis. 2013, 645379.

Baldaçara, L., Borgio, J.G.F., Lacerda, A.L.Td, Jackowski, A.P., 2008. Cerebellum and psychiatric disorders. Braz. J. Psychiatry 30, 281–289.

von Bartheld, C.S., 2012. Distribution of particles in the z-axis of tissue sections: relevance for counting methods. NeuroQuantol. Interdiscip. J. Neurosci. Quantum Phys. 10, 66–75.

Bost, M., Houdart, S., Oberli, M., Kalonji, E., Huneau, J.-F., Margaritis, I., 2016. Dietary copper and human health: current evidence and unresolved issues. J. Trace Elem. Med. Biol. 35, 107–115.

Deniz, Ö.G., Altun, G., Kaplan, A.A., Yurt, K.K., von Bartheld, C.S., Kaplan, S., 2018. A concise review of optical, physical and isotropic fractionator techniques in neuroscience studies, including recent developments. J. Neurosci. Methods 310, 45–53.

Desai, V., Kaler, S.G., 2008. Role of copper in human neurological disorders. Am. J. Clin. Nutr. 88, 855S–858S.

Gaggelli, E., Kozlowski, H., Valensin, D., Valensin, G., 2006. Copper homeostasis and neurodegenerative disorders (Alzheimer's, prion, and Parkinson's diseases and amyotrophic lateral sclerosis). Chem. Rev. 106, 1995–2044.

Guevara, C., Bulatova, K., Barker, G.J., Gonzalez, G., Crossley, N.A., Kempton, M.J., 2016. Whole-brain atrophy differences between progressive supranuclear palsy and idiopathic Parkinson's disease. Front. Aging Neurosci. 8, 218.

Gundersen, H., Bagger, P., Bendtsen, T., Evans, S., Korbo, L., Marcussen, N., Møller, A., Nielsen, K., Nyengaard, J., Pakkenberg, B., 1988. The new stereological tools: disector, fractionator, nucleator and point sampled intercepts and their use in pathological research and diagnosis. Apmis 96, 857–881.

Hordyjewska, A., Popiołek, Ł., Kocot, J., 2014. The many "faces" of copper in medicine and treatment. Biometals 27, 611–621.

Hyde, D.M., Tyler, N.K., Plopper, C.G., 2007. Morphometry of the respiratory tract: avoiding the sampling, size, orientation, and reference traps. Toxicol. Pathol. 35, 41–48.

Kalita, J., Kumar, V., Misra, U.K., Bora, H.K., 2018. Memory and learning dysfunction following copper toxicity: biochemical and immunohistochemical basis. Mol. Neurobiol. 55, 3800–3811.
Kapkaeva, M.R., Popova, O.V., Kondratenko, R.V., Rogozin, P.D., Genrikhs, E.E., Stelmashook, E.V., Skrebitsky, V.G., Khaspekov, L.G., Isaev, N.K., 2017. Effects of copper on viability and functional properties of hippocampal neurons in vitro. Exp. Toxicol. Pathol. 69, 259–264.
Kozma, M., Szerdahelyi, P., Kása, P., 1981. Histochemical detection of zinc and copper in various neurons of the central nervous system. Acta Histochem. 69, 12–17.
Kristiansen, S.L.B., Nyengaard, J.R., 2012. Digital stereology in neuropathology. Apmis 120, 327–340.
Madsen, E., Gitlin, J.D., 2007. Copper and iron disorders of the brain. Annu. Rev. Neurosci. 30, 317–337.
Monville, C., Torres, E.M., Dunnett, S.B., 2006. Comparison of incremental and accelerating protocols of the rotarod test for the assessment of motor deficits in the 6-OHDA model. J. Neurosci. Methods 158, 219–223.
Nakamura, Y., Gaetano, L., Matsushita, T., Anna, A., Sprenger, T., Radue, E.-W., Wuerfel, J., Bauer, L., Amann, M., Shinoda, K., 2018. A comparison of brain magnetic resonance imaging lesions in multiple sclerosis by race with reference to disability progression. J. Neuroinflamm. 15, 255.
Newhook, R., Hirtle, H., Byrne, K., Meek, M., 2003. Releases from copper smelters and refineries and zinc plants in Canada: human health exposure and risk characterization. Sci. Total Environ. 301, 23–41.
Noorafshan, A., Abdollahifar, M.-A., Karbalay-Doust, S., Asadi-Golshan, R., Rashidian-Rashidabadi, A., 2015. Sertraline and curcumin prevent stress-induced morphological changes of dendrites and neurons in the medial prefrontal cortex of rats. Folia Neuropathol. 53, 69–79.
Noorafshan, A., Hashemi, M., Karbalay-Doust, S., Karimi, F., 2018. High dose Allura Red, rather than the ADI dose, induces structural and behavioral changes in the medial prefrontal cortex of rats and taurine can protect it. Acta Histochem. 120, 586–594.
Opazo, C.M., Greenough, M.A., Bush, A.I., 2014. Copper: from neurotransmission to neuroproteostasis. Front. Aging Neurosci. 6, 143.
Özcelik, D., Uzun, H., Nazıroglu, M., 2012. N-acetylcysteine attenuates copper overload-induced oxidative injury in brain of rat. Biol. Trace Elem. Res. 147, 292–298.
Pal, A., Prasad, R., 2016. Regional distribution of copper, zinc and iron in brain of Wistar rat model for non-Wilsonian brain copper toxicosis. Indian J. Clin. Biochem. 31, 93–98.
Popescu, B.F.G., Robinson, C.A., Rajput, A., Rajput, A.H., Harder, S.L., Nichol, H., 2009. Iron, copper, and zinc distribution of the cerebellum. Cerebellum 8, 74–79.
Potera, C., 2004. Copper in Drinking Water: Using Symptoms of Exposure to Define Safety. National Institue of Environmental Health Sciences.
Przybyłkowski, A., Gromadzka, G., Wawer, A., Bulska, E., Jabłonka-Salach, K., Grygorowicz, T., Schnejder-Pachołek, A., Członkowski, A., 2013. Neurochemical and behavioral characteristics of toxic milk mice: an animal model of Wilson's disease. Neurochem. Res. 38, 2037–2045.
Ranjan, A., Kalita, J., Kumar, V., Misra, U., 2015. MRI and oxidative stress markers in neurological worsening of Wilson disease following penicillamine. Neurotoxicology 49, 45–49.
Royer, A., Sharman, T., 2020. Copper Toxicity, StatPearls [Internet]. StatPearls Publishing.
Sadiq, S., Ghazala, Z., Chowdhury, A., Büsselberg, D., 2012. Metal toxicity at the synapse: presynaptic, postsynaptic, and long-term effects. J. Toxicol. 2012, 132671.
Sathyanesan, A., Zhou, J., Scafidi, J., Heck, D.H., Sillitoe, R.V., Gallo, V., 2019. Emerging connections between cerebellar development, behaviour and complex brain disorders. Nat. Rev. Neurosci. 20, 298–313.
Schilsky, M.L., 2009. Wilson disease: current status and the future. Biochimie 91, 1278–1281.
Smolinski, L., Litwin, T., Redzia-Ogrodnik, B., Dziezyc, K., Kurkowska-Jastrzebska, I., Czlonkowska, A., 2019. Brain volume is related to neurological impairment and to copper overload in Wilson's disease. Neurol. Sci. 40, 2089–2095.
Squitti, R., Polimanti, R., 2013. Copper phenotype in Alzheimer's disease: dissecting the pathway. Am. J. Neurodegener. Dis. 2, 46–56.
Stezin, A., George, L., Jhunjhunwala, K., Lenka, A., Saini, J., Netravathi, M., Yadav, R., Pal, P.K., 2016. Exploring cortical atrophy and its clinical and biochemical correlates in Wilson's disease using voxel based morphometry. Parkinsonism Relat. Disord. 30, 52–57.
Tapiero, H., Townsend, D., Tew, K., 2003. Trace elements in human physiology and pathology. Copper. Biomed. Pharmacother. 57, 386–398.
Taylor, A.A., Tsuji, J.S., Garry, M.R., McArdle, M.E., Goodfellow, W.L., Adams, W.J., Menzie, C.A., 2020. Critical review of exposure and effects: implications for setting regulatory health criteria for ingested copper. Environ. Manag. 65, 131–159.
Terwel, D., Löschmann, Y.N., Schmidt, H.H.J., Schöler, H.R., Cantz, T., Heneka, M.T., 2011. Neuroinflammatory and behavioural changes in the Atp7B mutant mouse model of Wilson's disease. J. Neurochem. 118, 105–112.
Turgut, G., Akdogan, I., Adiguzel, E., Genç, O., 2003. Effect of copper overload together with ethanol uptake on hippocampal neurons. Tohoku J. Exp. Med. 199, 239–245.
Xu, T., Yu, X., Perlik, A.J., Tobin, W.F., Zweig, J.A., Tennant, K., Jones, T., Zuo, Y., 2009. Rapid formation and selective stabilization of synapses for enduring motor memories. Nature 462, 915–919.
Yang, G., Pan, F., Gan, W.-B., 2009. Stably maintained dendritic spines are associated with lifelong memories. Nature 462, 920–924.
van der Zee, E.A., 2015. Synapses, spines and kinases in mammalian learning and memory, and the impact of aging. Neurosci. Biobehav. Rev. 50, 77–85.